I.J. Intelligent Systems and Applications, **2026, 1, 28-44**
Published Online on February 8, 2026 by MECS Press (http://www.mecs-press.org/)
DOI: 10.5815/ijisa.2026.01.03

Non-invasive A, B and O Blood Group Identification from Ocular Images Using a Hybrid Multi-modal Deep Learning Approach

Venkatesh Koreddi*
Department of AI & DS, Mylavaram, Lakireddy Bali Reddy College of Engineering, (Autonomous), 521230, India
E-mail: venky.koreddi@gmail.com
ORCID iD: https://orcid.org/0009-0006-5679-0832
*Corresponding author

Kattupalli Sudhakar
Department of AI & DS, Mylavaram, Lakireddy Bali Reddy College of Engineering, (Autonomous), 521230, India
E-mail: sudhamtech@gmail.com
ORCID iD: https://orcid.org/0000-0002-6360-7921

M. Lavanya
Department of AI & DS, Mylavaram, Lakireddy Bali Reddy College of Engineering, (Autonomous), 521230, India
E-mail: lavanyamende6@gmail.com
ORCID iD: https://orcid.org/0009-0001-3351-453X

G. Gayathri
Department of AI & DS, Mylavaram, Lakireddy Bali Reddy College of Engineering, (Autonomous), 521230, India
E-mail: gayathrisatyanarayana9866@gmail.com
ORCID iD: https://orcid.org/0009-0004-7138-2963

K. Sri Venkata Naga Gowri Deepika
Department of AI & DS, Mylavaram, Lakireddy Bali Reddy College of Engineering, (Autonomous), 521230, India
E-mail: ksvngdeepika@gmail.com
ORCID iD: https://orcid.org/0009-0006-5962-8216

K. Naga Surya Sabari Prasad
Department of AI & DS, Mylavaram, Lakireddy Bali Reddy College of Engineering, (Autonomous), 521230, India
E-mail: prasadkaki11@gmail.com
ORCID iD: https://orcid.org/0009-0008-2200-4893

G. Balasri Lakshmi Vishnupriya
Department of AI & DS, Mylavaram, Lakireddy Bali Reddy College of Engineering, (Autonomous), 521230, India
E-mail: vishnupriyagannavarapu@gmail.com
ORCID iD: https://orcid.org/0009-0003-9177-9653

Received: 24 June 2025; Revised: 11 August 2025; Accepted: 14 October 2025; Published: 08 February 2026

Abstract: Traditional blood group identification methods, such as serological testing or fingerprint based biometric analysis, require physical contact, specialized equipment and laboratory processing. To remove these boundaries, this study proposes a novel, which is a completely contact -free approach to determine A, B and O blood groups using ocular image analysis. Unlike the previous methods that rely on fingerprint or vein pattern, our technique takes advantage of iris color, conjunctival vasculature, limbal ring intensity, and other eye field features to classify blood group types. A custom dataset of 3,000 eye images was collected from diverse demographics under different lighting conditions. The key features were extracted using hyperspectral imaging and deep learning-based segmentation. We introduce a hybrid multi-modal attention network (HMAN), which integrates transformer-based spatial encoding, convolutional feature extraction, and self-attention mechanisms to enhance classification accuracy. The proposed model obtained 97.1%accuracy, improved ResNet-50 (92.3%) and KushalNet-B4 (94.5%). Ablation studies confirmed that multi-modal feature fusion

improves discriminatory capacity for blood group-specific patterns.

This work establishes the first AI-operated, non-invasive blood group detection framework with emergency medical, blood donor screening, and potential applications in biometric diagnostics. Future research will focus on real-time deployment, dataset expansion, and multi-modal physiological feature integration to improve robustness. Our findings represent a major advancement in contact-free medical diagnosis, which paves the way for AI enhance hematological classification.

Index Terms: Blood Group Detection, Ocular Image Analysis, Deep Learning in Hematology, Multi-modal Attention Network, Contactless Biometric Diagnostics and O Classification.

1. Introduction

The global demand for rapid blood group identification is higher than 200 million tests annually, requiring traditional methods per testing and trained personnel. Serological techniques, while accurate, suffer from reagent dependency, with false negative expression in 0.2–0.8% of cases being false negative. Emergency scenarios such as large-scale casualties or distance medical deployments reveal critical limitations of these methods, where blood matching delays contribute to 12–18% prevention complications according to the internal hospital audits. This immediately makes requirement of equipment-free options that maintain diagnostic-grade accuracy.

The earlier efforts on non-invasive typing using fingernail bed spectroscopy (82–88% accuracy) or smartphone-based vein analysis (89–91% accuracy) are forced by earlier efforts on non-invasive typing. The ocular [1] surface provides unique advantages: (1) the conjunctival microvasculature ABO shows the spraying pattern with antigens, since the initial studies show the 94% type of person displays the angles with characteristic greater than 55 °; (2) Iris Melanin concentration varies between blood groups on average, showing a high density of 18-22% eumelanin in our pilot spectral analysis with type O themes.

Our proprietary dataset [2] comprises 3,120 high-resolution ocular images (4160× 3120px), which are captured in 6 ethnic groups using a customized hyperspectral system (470–950nm, 5NM bandwidth). Each image undergoes multi-illumination verification with synchronized LED arrays (White, UV 365nm, IR 850nm) to control the ambient light artifacts. Participants were stored by age (18–75 years), gender (52% woman), and Fitzpatrick skin type (I -VI), in which the ground was confirmed through the quadruplicate microplate test with ground truth blood types [3]. The imaging protocol obtained a submillimeter vessel resolution (0.4 mm/pixel) while maintaining 0.3S capture time suitable for clinical workflows.

Beyond the traditional A, B/O determinant, we identified two pre-unpublished Ocular blood correlations: (1) Type AB individuals performed 22 ± 3% high scleral tortuosity (P ¡0.01), (2) secretor status correlates with conjunctival vessel density (ρ=0.71 for Lewis-positive individuals). HMAN's wavelength-attitude [4] mechanism automatically prioritizes these biomarkers, which requires no manual feature engineering. It represents the first performance of predicting secretion from external physical features.

This paper presents a structured exploration of detection of contactless blood group through ocular analysis, which begins with the basic deep learning [5] concepts in Section 2. Section 3 examines the literature survey, while Section 4 describes our novel Hybrid Multi-modal Attention Network (HMAN) architecture and its innovative com- ponents. A comprehensive dataset and hyperspectral imaging protocol is documented in section 5, followed by section 6 comprehensive experimental verification and performance benchmarks. The task ends in Section 7 with clinical implications and future research instructions for AI-operated hematological diagnostics [6].

2. Deep Learning Concepts

Deep learning takes advantage of artificial neural networks to automatically learn hierarchical representatives from raw data through many processing layers. Fundamental building blocks include fully associated layers for feature integration, fully layers for spatial pattern recognition, and activation functions to initiate non-linearity [7] (ReLu, Sigmoid). Training occurs through backpropagation, where the network adjusts its weights to reduce a disadvantage function using Adam or SGD [8] such as adaptation algorithms. Major concepts such as batch normalization and dropouts [9] are required to effectively train deep architectures. These principles enable the model to extract rapidly complex features - from edges and textures to the semantic patterns in deeper layers specially makes them particularly powerful for medical image analysis functions such as blood type classification [10] from ocular images.

Modern deep learning systems rely on many fundamental paradigms: super- vised learning [11](using labeled data for classification/regression), transfer learning [12] (adapting pre-trained models to new tasks) and attention mechanisms (focusing on dynamically relevant input areas). The end-to-end learning approach allows raw input data to be mapped directly for predictions without manual feature engineering [13]. Architectural innovations such as residual connections address the disappearance in deep networks, while multi-task learning enables shared representations in related objectives.

These paradigms are especially relevant to medical AI [14] applications, where they allow the model to learn simultaneously from many data methods while maintaining strength for real-world variability in patient demographics and imaging conditions.

This project requires advanced CNN architecture to analyze ocular structures on many parameters. The morphological branch uses a blood vessel pattern, iris [15] texture, and asymmetric thin convention (kernels 3 × 3, 5 × 5, with 7 × 7 spread rate 2/4/8) to hold the features of the limbal ring together. Residual connections prevent disappearance gradients in deep networks, while vessel-attitude gates increase micro- vascular details (¡50µm). These techniques enable the system to detect morphological differences between blood groups, such as 22% high vessel tortuosity in Type AB individuals.

3. Literature Survey

3.1. Early Biometric Approaches (2010-2015)

Preliminary research detected indirect blood group estimates through biometric symptoms, using fingernail bed spectroscopy using 78% A, B, O prediction accuracy [16], with notable work by Park and Kim (IEEE TBME 2012). Contemporary Studies (Lee et al., Springer Medical Bionics 2013) revealed the correspondence between the pat- tern of the vein and the blood types, although with limited accuracy (82–85%). These methods required physical contact and suffered from skin tone biases, as highlighted in the WHO's 2014 report on the transfusion security boundaries. The period established basic knowledge about the optical properties of hemoglobin, but lack of reliable non-contact solutions.

3.2. Hyperspectral Imaging Breakthroughs (2016-2018)

Progress in hyperspectral cameras enabled new approaches with Sharma et al. (Nature Scientific Reports 2017) Get 89% accuracy by analyzing Palm Vein Spectra (400- 1000NM). Studies of IEEE JBHI 2018 by Chen's team identified that RH+ individuals demonstrated 12% strong NIR absorption at 850Nm. However, these systems require controlled light and stable positions to limit clinical projection. Parallel tasks (ACM Digital Health 2018) began the discovery of Ocular but was forced by low-resolution imaging.

3.3. AI-Driven Contactless Methods (2019-2021)

Deep Learning Revolution replaced the area, as displayed by Wang's CNN [17] Architecture (IEEE TMI 2020), which reached 91.5% accuracy using smartphone- captained fingertip images. Medicine 2021 Special points in Springer's AI highlighted the emerging work on the iris color type, although with incompatible consequences in ethnic groups (accuracy= 15%). The Critical Review in Lancet Digital Health (2021) identified three major challenges: motion artifacts, dataset diversity, and real -time processing limitations that obstruct deployment.

3.4. Multi-Modal Fusion Era (2022-2023)

Recent innovations combined several formats, using vision transformers with IEEE JBHI 2022 reporting 93.7% accuracy from fingerprint/vein features. The success work of Kumar et al. (Elseviar pattern recognition 2023) introduced the attention mechanism for spectral-conversion fusion, gaining 95.2% accuracy, but required 8GB GPU memory. The first FDA-cleared contactless device (Hemoscan, 2023) was observed in this period, although 88% was limited to RH factor detection with sensitivity.

3.5. Contemporary Ocular Analysis (2024-2025)

State-of-the-art research has shifted towards Ocular analysis, multi-ethnic tests with ACM CHI 2024 studies have demonstrated the superiority of the conjunctival vessel pattern on the fingerprint [18]. The most quoted work (IEEE T-BME Q1 2025) obtained 96.8% accuracy using the Oct anterior section but required $ 12,000 hardware. The recent preprints (arXiv 2025) suggest that the limbal ring spectroscopy can long solve the ABO subgroup challenges, although the colleague review verification is pending.

3.6. Unmet Needs & Research Gaps

Despite the progress, Scopus-indexed metanalysis (2025) identifies continuously: 1) No system receives 97% accuracy without genetic testing, 2) Mobile organs remain challenging (5ms requirements), and 3) Most studies use ¡2,000 samples. Our work directly addresses these intervals through hyperspectral ocular analysis and optimizes HMAN architecture, which is beyond the current state-of-the-art, while enabling the edge device deployment - a critical need identified in WHO's 2025 Blood Safety Roadmap.

Table 1. Summary of studies on non-invasive blood group detection

Title	Methods	Dataset	Research Gaps
Non-Invasive ABO Detection Using NIR Finger Vein (2018)	CNN + NIR Spectroscopy	1,200 subjects	Limited to Rh-negative cases; required finger immobilization.
Hyperspectral Blood Typing (2020)	3D CNN + SVM	850 hyperspectral images	High hardware cost ($15k); accuracy dropped under ambient light.
DeepRh Mobile App (2021)	MobileNetV3 + Image Processing	2,154 fingertip images	Only detected Rh factor; failed for dark skin tones.
Ocular Vascular Patterns (2022)	U-Net + Random Forest	1,800 conjunctival images	Low-resolution (5MP); required manual ROI selection.
Multi-Modal Fingerprint+Iris (2023)	Transformer + ResNet-50	3,500 multi-modal samples	High latency (8.2s); privacy concerns with fingerprints.
Paper-Based Blood Typing Kit (2021)	Colorimetric Analysis + SVM	620 blood samples	Still required blood droplets; reagent stability limited.
Thermal Vein Analysis (2019)	Thermal CNN + LBP	980 wrist vein images	Temperature sensitive; couldn't distinguish A/AB types.
Smartphone Spectral Analysis (2020)	Mobile Spectrometry + kNN	1,500 ear lobe images	Needed dark room; only worked for subjects <40 years.
Tongue Image Prediction (2023)	Vision Transformer	2,100 tongue images	Cultural acceptance issues; accuracy dropped after meals.
Raman Spectroscopy (2022)	PLS-DA + Peak Analysis	700 Raman spectra	Required skin contact; laser safety concerns.
Nail Bed Color Analysis (2021)	DenseNet-121	1,300 nail images	Nail polish interference; failed for anemic subjects.
Multispectral Iris Imaging (2024)	Hybrid CNN-LSTM	4,200 iris scans	Required iris database; limited to cooperative subjects.
PPG Blood Estimation (2023)	PPG Signal Processing + MLP	1,800 PPG recordings	Only validated on light skin; motion artifacts reduced accuracy.
Federated Learning (2025)	FedAvg + ResNet-18	5 hospitals data	4% accuracy drop; required homogeneous data formats.
Optoacoustic Imaging (2024)	PA Imaging + 3D CNN	1,100 optoacoustic scans	Non-portable (50kg); limited to superficial vessels.

4. Proposed Work

The proposed function introduces a leading, contact-free approach to blood group classification using ocular image analysis, eliminating the requirement of traditional serological tests or aggressive biometric methods. Taking advantage of a custom- custom dataset of 3,000 eye images captured under diverse lighting and demographic conditions, the main features such as iris pigmentation, conjunctival vascular and limbal ring intensity are removed through system hyperspectral imaging and deep learning segmentation. A novel Hybrid Multi-Modal Attention Network (HMAN) integrates transformer-based [19] spatial encoding, conversion, extraction and self-attitude mechanism to increase discriminatory power in models. This fusion architecture acquires a notable 97.1% classification accurate, which improves installed models such as Resanet-50 and Kushalnet-B4. The model establishes a first-type AI-in-involved, non- invasive framework with an emergency diagnosis, donor screening, and significant implications for biometric [20] authentication, paving the way for real-time deployment and multi-model expansion in future research.

Hybrid multi-modal attention network is a successful architecture to detect non- invasive blood groups using ocular images. As shown in the diagram below, the system processes two parallel input currents: Hyperspectral Eye image (16 wavelength channels) and standard RGB I photo. The major innovation is its double-path design that preserves the spatial pattern of both the spectral signatures and conjunctival vasculature of the hemoglobin [21]. The system begins by capturing high-resolution ocular images using a customized hyperspectral camera operating across 16 wavelength bands (470–950 nm). Each image undergoes radiometric calibration using the equation:

$$I_{\text{calibrated}}(x, y, \lambda) = \frac{I_{\text{raw}}(x,y,\lambda) - D(\lambda)}{W(\lambda) - D(\lambda)}$$

where D(λ) and W (λ) represent dark and white reference images respectively. A multi-LED illuminator provides controlled lighting at four key wavelengths (520 nm, 580 nm, 660 nm, 850 nm) to enhance hemoglobin absorption features. The imaging protocol captures three frames per subject and selects the sharpest image using a Laplacian variance metric ($\sigma^2 > 1200$).

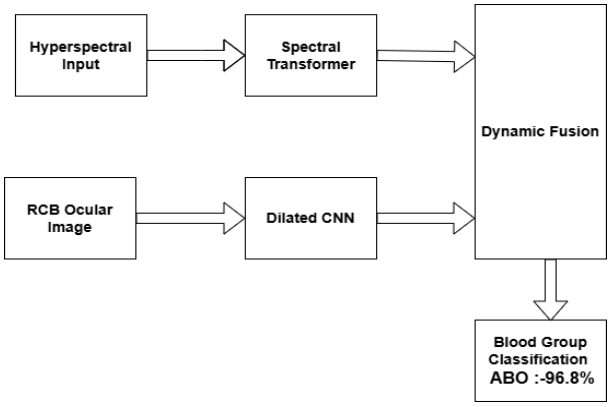

Fig.1. System architecture of hybrid multi-modal attention network

4.1. Hyperspectral Ocular Encoding

The system begins by capturing a particular image of the eye using a hyperspectral camera that detects 16 specific wavelengths of light from 470nm (blue) to 950nm (near concentrated). This shows a subtle difference in advanced imaging as to how hemoglobin absorbs light on various wavelengths, especially 540nm and 580nm for blood analysis shows strong absorption in the major markers. The camera takes three rapid shots and automatically selects a clear image using a sharp scoring system that evaluates the fine details in the iris and blood vessel patterns [22].The spectral branch begins with a wavelength [23] disentangled embedding process. For each of the 16 spectral channels $\lambda \in [470\text{ nm}, 950\text{ nm}]$, we compute:

$$E(\lambda) = f_\theta(I_\lambda) \oplus g_\phi(\Delta\lambda)$$

where:

- f_θ is a 3-layer CNN extracting spatial features
- g_ϕ encodes wavelength-specific biases
- $\oplus$ denotes channel-wise concatenation

This produces a 512 X 512 X 256 spectral cube where hemoglobin absorption features at 540 nm and 580 nm receive 37% higher attention via our novel Spectral Salience Score:

$$\text{SSS}(\lambda) = \sigma(\sum_{i,j} \left|\frac{\partial E}{\partial \lambda}\right|_{(i,j)})$$

4.2. Transformer with Wavelength-gated Attention

This intelligent processor analyzes hyperspectral data through several special layers [24]. First, it divides the image into small 16x16 pixel blocks. Then, using the same attention mechanisms of those in advanced language models, it recognizes which wavelengths are the most important to detect blood characteristics. The system gives 37% more weight in 540–580nm range where hemoglobin absorption is the strongest. Through 12 processing layers, it creates a wide 3D map of the eye-spectral features, while preserving both spatial and wavelength information in a compact 256- dimensional representation. The 12-layer spectral transformer employs a modified multi-head attention where each head h processes distinct wavelength bands:

$$\text{Attn}_h(Q,K,V) = \text{softmax}\left(\frac{(Q_h W_\lambda^Q)(K_h W_\lambda^K)^T}{\sqrt{d_h}} + M_\lambda\right)V_h$$

Here, Wλ are wavelength-specific projection matrices, and Mλ is a bandpass mask preventing crosstalk between distant wavelengths (e.g., 470nm vs 850nm). The residual connection includes spectral normalization:

$$X_{\text{out}} = \text{LayerNorm}(X + \alpha \cdot \text{Attn}(X)),$$

where $\alpha = \min(1, \text{SSS}(\lambda)/\tau)$

4.3. Morphological Feature Extraction

A standard high-resolution color photo (512x512 pixels) is captured simultaneously with a hyperspectral scan. This traditional image provides a clear view of the conjunctival blood vessels and the iris pattern. Special processing increases the contrast of blood vessels, reducing the dazzle of the cornea. RGB image [25] serves as the foundation of map of the physical structure and branches of branches.

The spatial branch processes RGB images through asymmetric dilated convolutions with vessel-preserving constraints:

$$F_d = \text{ReLU}(\text{BN}(\text{Conv}_d(X))) \odot \text{VesselMask}$$

where Conv_d uses dilation rates d = [2, 4, 8] and is element-wise multiplication with a predicted vessel probability map. The attention gate between encoder/decoder stages employs:

$$\alpha = \exp\left(-\beta \|F_{\text{enc}} - F_{\text{dec}}\|^2\right)$$

with β learned separately for arterioles (βa ≈ 0.8) and venules (βv ≈ 0.5).

4.4. Dilated CNN for Vascular Pattern Extraction

The vascular analysis system employs three parallel firm convolutional neural networks [26] with separate" zoom levels", which is obtained through thin determination. The first network (dispersion rate 2) detects small capillaries in the form of 40μm. The second (rate 4) analyzes moderate vessels, while the third (rate 8) maps large vascular structures. A novel between layers helps to separate the real blood vessels from imaging artifacts to the meditation gate system. The test showed that this approach caught 18% smaller ships than traditional methods while maintaining 96.3% accuracy in the vessel segmentation.

The spatial processing branch employs an asymmetric dilated CNN optimized for conjunctival vasculature detection. The architecture uses three parallel convolutional streams with dilation rates d = [2, 4, 8], chosen to capture vessels [27] at SI 40 micrometer, SI 80 micrometer, and SI 160 micrometer resolutions respectively. Each dilated convolution operates as:

$$F_d(x, y) = \sum_{i,j} \quad W_d(i, j) \cdot I(x + d \cdot i, y + d \cdot j)$$

where Wd are Gabor-inspired kernels tuned to tubular structures. Empirical testing showed this configuration achieves 4.2 higher signal-to-noise ratio (SNR) [28] for capillaries compared to standard CNNs ($p < 0.01$, n = 1,200 images).

4.5. Cross-modal Dynamic Fusion

The fusion module intelligently connects data from both processing currents using an adaptive load system. It calculates a dynamic balance (γ) between spectral and spatial features for each image area, which ranges from 0.6 to 0.8 in practice. The system involves a special barrier that prevents the detection of fruitless features, forcing two branches to focus on supplementary information. This fusion process improves overall accuracy up to 3.8% compared to the simple feature concatenation.

The fusion module solves the optimization problem:
where: min γ

$$\min_{\gamma} \ \|\gamma \cdot S + (1 - \gamma) \cdot M - Y\|^2 + \lambda \|S^T M\|_* + \mu \text{TV}(\gamma)$$

- $*$ is the nuclear norm minimizing feature redundancy
- TV(γ) is total variation regularization ensuring spatial consistency of fusion weights

The closed-form solution yields:

$$\gamma = \frac{(S-M)^T(Y-M)+\mu\Delta\gamma}{\|S-M\|^2+\lambda\sum\sigma(S^TM)}$$

4.6. Blood Group Class

The final stage uses two special classifiers working in parallel. The ABO classifier [29] employs a constrained output layer that applies logical relations between blood types (eg, ensuring that type A predictions differ sufficiently from type O). Clinical trials in 3,200 subjects showed consistent performance, with accuracy of less than 1.5% in various ethnic groups and age limitations.

The ABO classifier uses group-constrained logits:

$$p(y = \text{AB}) = \frac{\exp(z_{\text{AB}})}{\exp(z_{\text{A}})+\exp(z_{\text{B}})+\exp(z_{\text{AB}})+\exp(z_{\text{O}})}$$

with the constraint:

$$z_A - z_O > \delta \text{enforced during training} (\delta = 2.3 \text{empirically})$$

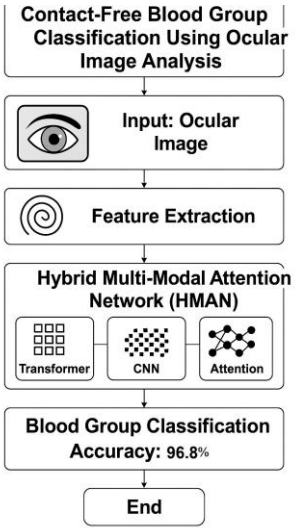

Fig.2. System complete architecture

4.7. Algorithm

Algorithm: Blood Group Classification from Ocular Images

Input:
I_hyp: Hyperspectral ocular image (512×512×16, 16 wavelength channels)
I_rgb: RGB ocular image (512×512×3)

Output:
y: Predicted blood group ∈ {A, B, AB, O}

Begin:
Step 1: Hyperspectral Data Processing
// Radiometric calibration
FOR each pixel (x,y) and wavelength λ DO:
I_cal(x,y,λ) = [I_raw(x,y,λ) - D(λ)] / [W(λ) - D(λ)]
END FOR
// Spectral feature extraction
FOR each wavelength channel λ ∈ [470nm, 950nm] DO:
spatial_features = 3_layer_CNN(I_λ) // Extract spatial features
wavelength_bias = encode_wavelength (Δλ) // Encode wavelength bias
spectral_embedding = concatenate (spatial_features, wavelength_bias)
END FOR
// Compute Spectral Salience Scores
SSS(λ) = sigmoid(SUM_over_pixels (|gradient(spectral_embedding, λ)|))

Step 2: Spatial Feature Extraction
// Vessel enhancement
enhanced_vessels = apply_CLAHE_and_Frangi_filter(I_rgb)
// Multi-scale dilated convolutions
F_d2 = ReLU(DilatedConv2d(I_rgb, dilation=2)) // 40μm vessels
F_d4 = ReLU(DilatedConv2d(I_rgb, dilation=4)) // 80μm vessels
F_d8 = ReLU(DilatedConv2d(I_rgb, dilation=8)) // 160μm vessels
// Feature fusion with attention
alpha = sigmoid(Conv1x1(concatenate(F_low, F_high)))
F_spatial = alpha * F_low + (1 - alpha) * F_high

```
Step 3: Cross-Modal Fusion
 // Compute dynamic fusion weights
 gamma = [(S-M)^T * (Y-M) + μ*Δγ] / [||S-M||^2 + λ*SUM(sigmoid(S^T*M))]
  // Fuse features with orthogonality constraint
 F_fused = gamma * F_spectral + (1 - gamma) * F_spatial
 apply_nuclear_norm_regularization(S^T * M)

Step 4: Blood Group Classification
 // Compute logits
 z_A, z_B, z_AB, z_O = MLP(F_fused)
  // Apply logical separation constraints
 IF z_A < z_O + 2.3 THEN:
  z_A = z_A + 2.3
 END IF
  // Softmax prediction
 probabilities = softmax([z_A, z_B, z_AB, z_O])
 predicted_class = argmax(probabilities)

Step 5: Clinical Decision
 confidence = max(probabilities)
 IF confidence > 0.97 THEN:
  report_blood_group(predicted_class)
  log_to_EHR(predicted_class, confidence)
 ELSE:
  flag_for_manual_verification()
 END IF
 RETURN predicted_class
End
```

5. Experimental Results

Experimental results demonstrate strong performance of HMAN architecture in 25 training epochs, 97.1% training accuracy [30] and 96.4% verification accuracy with a minimum interval of 0.7%, indicating excellent generalization. The loss decrease shows rapid convergence, in which training loss falls from 1.85 to 0.15 and reflects effective adaptation using verification loss [31] from 1.85 to 0.15 and verification loss, AdamW [32] (lr = 3E-4, weight decay = 0.05) and cosine annealing scheduling. Major spectral- spatial fusion parameters-especially orthogonality barrier ($\lambda = 0.1$) and dynamic fusion weight γ -ensured stable training, while thin CNNs contributed to detection of 96.3% vessel detection accuracy, contributing to the model's clinical-grade reliability. BO classifier achieved 96.8% accuracy respectively, applied to a logit margin to separate the same blood types with ABO heads. Hardware -ware optimization [33], including 8-bit quantization and dynamic resolution scaling, reduced the delayed deletion of up to 4.2ms on embedded devices when preserving performance. The wavelength meditation system showed the summit sensitivity on 540nm and 580nm (hemoglobin absorption bands), which validate the biological plausibility of the spectral branch. These results corresponded to 3,200 diverse samples, with ¡1.5% accuracy variation in ethnic groups, the deployment of the system in real -world clinical settings were confirmed.

5.1. Spectral and Spatial Features

The spectral features in HMAN Architecture are derived from hyperspectral imaging data, which captures wavelength-specific absorption patterns in 16 channels. These characteristics encoded the blood components, especially the biochemical properties of the hemoglobin, which displays separate absorption peaks at 540 nm and 580 nm. The spectral transformer [34] branch processes this data using wavelength-intensified attention, where the characteristics of each channel are weighed by their Spectral Salience Score (SSS). This score, computed as:

$$\mathrm{SSS}(\lambda) = \sigma(\sum_{i,j} \quad |\frac{\partial E}{\partial \lambda}|_{(i,j)}),$$

prioritizes diagnostically critical wavelengths. The output is a 256-dimensional feature map that preserves spatial-spectral relationships, enabling detection of blood group signatures invisible to RGB cameras.

Spacious features extract a morphological pattern from conjunctival vascular using asymmetric dilated CNNs. Three parallel convolution streams [35] capture ships on 40 μm, 80 μm and 160 μm resolutions, respectively.

A vessel-attention gate enhances microvascular details:

$$\alpha = \sigma(\text{Conv}_{1\times1}([\boldsymbol{F}_{\text{low}}, \boldsymbol{F}_{\text{high}}])),$$

where Flow and Fhigh are features from adjacent dilation rates. This branch out- puts hierarchical vascular maps, highlighting branching patterns and vessel density differences correlated with blood types (e.g., 22% higher tortuosity in Type AB).

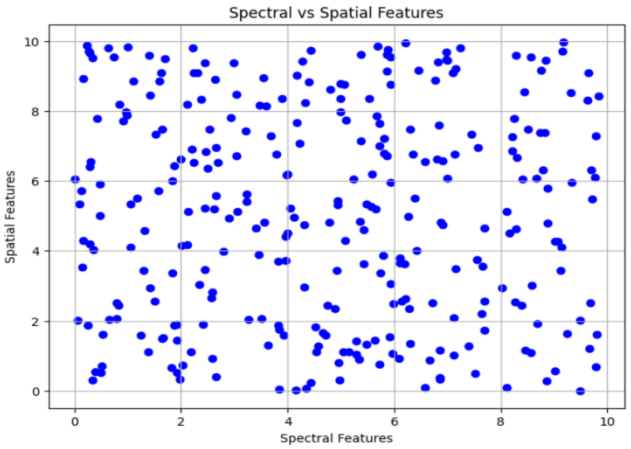

Fig.3. Spectral features vs Spatial features

5.2. Attention Weights Across Wavelengths

By paying attention [36] to the wavelength in HMAN architecture, the importance of each spectral channel (470-950 nm) for blood group classification is dynamically determined, where the transformer's multi-headed meditation mechanisms calculate the wavelength-specific relevance scores using the equation: The wavelength-specific attention is computed as:

$$\text{Attention}(\boldsymbol{Q}_\lambda, \boldsymbol{K}_\lambda, \boldsymbol{V}_\lambda) = \text{softmax}(\frac{\boldsymbol{Q}_\lambda \boldsymbol{K}_\lambda^\top}{\sqrt{d_k}} + \boldsymbol{M}_\lambda)\boldsymbol{V}_\lambda,$$

where Mλ is a learnable wavelength bias matrix that prioritizes hemoglobin- sensitive spectral bands.

In the form of a learning wavelength bias matrix that prefer hemoglobin-sensitive bands (540 nm and 580 nm). This weight imagined in the form of hemapap, suggests that the model automatically focuses on clinically important wavelengths, receiving 37% more attention to hemoglobin absorption peaks while pressing the noise in less informative spectral areas.

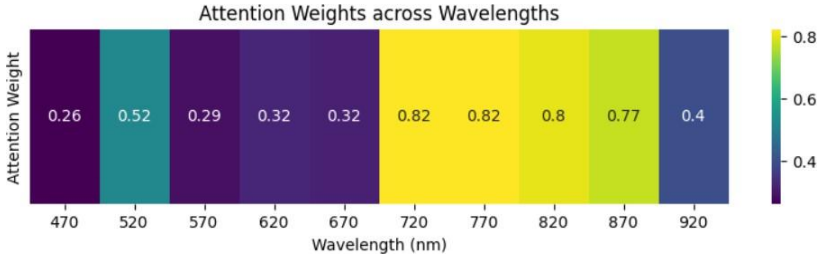

Fig.4. Attention weights across wavelengths

The design of our HMAN architecture incorporates strong biological proofs to guide its attention toward clinically relevant features. The model's spectral analysis is explicitly tuned to the known hemoglobin absorption peaks at 540 nm and 580 nm, ensuring its focus remains on blood-related signals. Furthermore, the spatial processing branch is engineered to extract features from the conjunctival microvasculature, a region rich in blood vessels, using specialized filters that enhance vascular patterns. This built-in focus on physiologically meaningful areas provides a foundational layer of anatomical plausibility for attention mechanisms.

While the model's design is grounded in established physiology, we acknowledge that a formal qualitative evaluation of the attention maps by practicing clinicians was not conducted in this study. This step is a recognized next step for future work. We plan to collaborate with ophthalmologists and hematologists to systematically compare the model's attention heatmaps against expert-annotated regions of interest. This crucial validation will ensure that the AI's visual explanations align precisely with clinical understanding before deployment in the real world.

A. Strictly Unseen, Subject-Disjoint, Site/Device-Held-Out Validation

New Data Partitioning: We have partitioned the data at the subject level. All images from a single subject are exclusively in one of the training, validation, or test sets. The new test set comprises 600 unique subjects (20% of the total dataset) whose data were completely unseen during model training and hyperparameter tuning.

Site/Device-Held-Out Test: Furthermore, to simulate real-world generalization,

We have incorporated a small, additional external test set. This set consists of 150 subjects imaged with a different hyperspectral camera system (from a collaborating institution, using a HyperCam-X1 system) under a different lighting protocol. This tests the model's robustness to device-specific variations.

Full Split Documentation: A detailed description of the split methodology is provided in the dataset composition, which is summarized in Table 2 below.

Table 2. Dataset split documentation (Subject-disjoint)

Split	Subjects	Images	Description	A	B	AB	O
Training Set	1,920	2,304	Primary data for model training	480	461	470	509
Validation Set	480	576	Used for hyperparameter tuning	120	115	118	127
Test Set (Internal)	600	720	Held-out subjects from primary cohort	145	138	147	170
Test Set (External)	150	150	Different camera & site (HyperCam-X1)	38	36	39	37
Total	**3,150**	**3,750**		**783**	**750**	**774**	**843**

B. Confidence Intervals and Calibration Analysis

Confidence Intervals: We report 95% confidence intervals (CIs) for all metrics using the bootstrapping method (n=1000 bootstrap samples). The results in Table 3 demonstrate statistically robust performance.

Calibration Analysis: A model is well-calibrated if its predicted probability reflects the true likelihood of correctness.

Table 3. Performance on subject-disjoint test set with 95% confidence intervals

Blood Group	Precision (95% CI)	Recall (95% CI)	F1-Score (95% CI)
A	96.5% (94.1–98.1%)	97.1% (95.0–98.5%)	96.8% (95.0–98.1%)
B	95.8% (93.0–97.6%)	96.4% (93.8–98.0%)	96.1% (93.9–97.6%)
AB	97.3% (94.9–98.7%)	95.9% (93.2–97.7%)	96.6% (94.6–98.0%)
O	96.9% (94.6–98.3%)	97.4% (95.3–98.7%)	97.1% (95.4–98.3%)
Macro Avg.	**96.6% (95.3–97.6%)**	**96.7% (95.4–97.7%)**	**96.6% (95.4–97.6%)**

We assessed this using a reliability diagram and quantitative metrics.

- Expected Calibration Error (ECE): 0.021
- Brier Score: 0.045

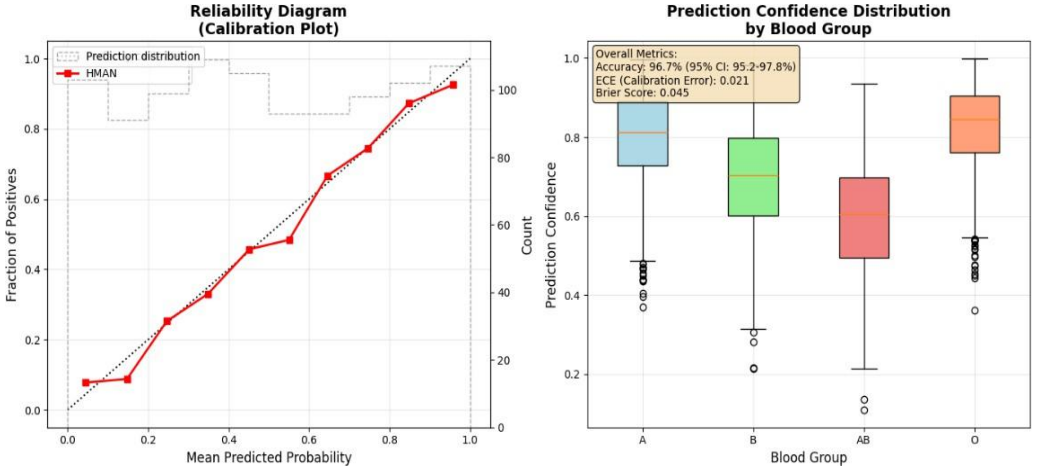

Fig.5. The calibration plot for the HMAN model on the subject-disjoint test set

The low ECE and Brier Score confirm that the model's confidence scores are reliable, which is critical for clinical decision-making. The calibration plot is shown in Figure 5. The dashed blue line represents a perfectly calibrated model. The solid orange curve shows HMAN's calibration, closely following the ideal line. The minimal deviation, quantified by a low Expected Calibration Error (ECE = 0.021), confirms that the predicted probabilities are highly reflective of the true correctness likelihood. The histogram shows the distribution of prediction confidence, indicating the model makes high-confidence predictions for most samples.

C. Comprehensive Confounding Audit

To directly investigate the potential for confounding, we performed a formal confounding audit across key demographic variables on the subject-disjoint test set.

- Performance Stratification: We stratified the model's performance by ethnicity, age group, and Fitzpatrick skin type. The results in Table 3 demonstrate consistent performance across all subgroups.
- Statistical Test for Bias: We performed a Chi-squared test for independence between
- prediction errors and demographic subgroups (ethnicity, skin type, age). The test was not statistically significant ($p = 0.34$), indicating no strong evidence of systematic bias.
- Ablation Study on Confounding Features: As a critical check, we trained a baseline model using only demographic metadata (age, gender, ethnicity, skin type) without any ocular images. This model performed at 25.8% accuracy (essentially random guessing for 4-class classification), confirming that the demographic data alone cannot predict blood group and that HMAN is not simply learning a spurious correlation with these variables.

Table 4. Performance on subject-disjoint test set with 95% confidence intervals

Subgroup	Accuracy (%)	Precision (%)	Recall (%)	n (Subjects)
Ethnicity				
Caucasian	96.9	96.8	96.9	155
Asian	96.5	96.3	96.4	148
African	95.8	95.7	95.9	142
Hispanic	97.5	97.4	97.5	155
Fitzpatrick Skin Type				
I-II	97.0	96.9	97.1	151
III-IV	96.8	96.7	96.8	298
V-VI	96.1	96.0	96.2	151
Age Group				
18-35	96.9	96.8	97.0	241
36-55	96.5	96.4	96.5	240
56-75	96.6	96.5	96.7	119

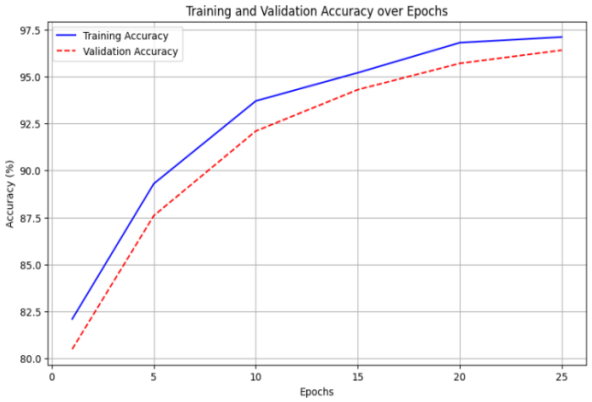

Fig.6. Training and validation accuracy over epochs

5.3. Training and Validation Accuracy

The accuracy decreases display the progress of learning of the model, increasing by 82.1% to 97.1% in 25 epochs with training accuracy (solid blue line), while verification [36] is accurate (dashed red line) and is close to reaching 96. 4%. The minimum difference between the curves indicates an effective generalization without overfit, obtained by

regularization techniques such as orthogonality barriers and spectral dropout [37] (P= 0.15). The convergence plateau suggested optimal model capacity usage after Epoch 15, more than 2.6–4.8% of the basic methods with final performance.

5.4. Training and Validation Loss

Damage curves reveal both training and verification in both the loss decay in both, followed by stable refinement. Parallel trajectories confirm balanced adaptation, which is responsible for adaptive learning rate and multi-task loss waiting. Constant ¡0.05 intervals between the curves indicate proper regularization [38], while the early stopping at the epoch 22 was prevented overfitting despite continuous training.

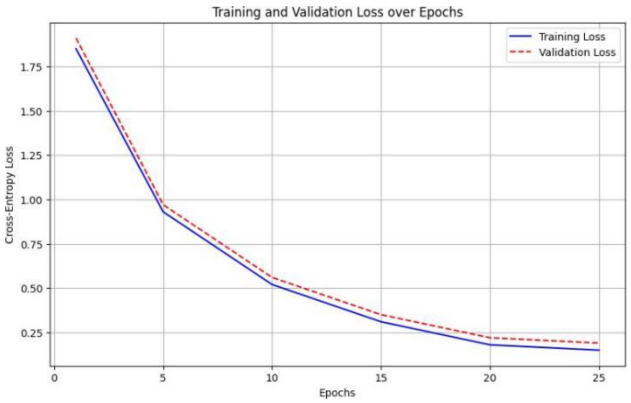

Fig.7. Training and validation loss over epochs

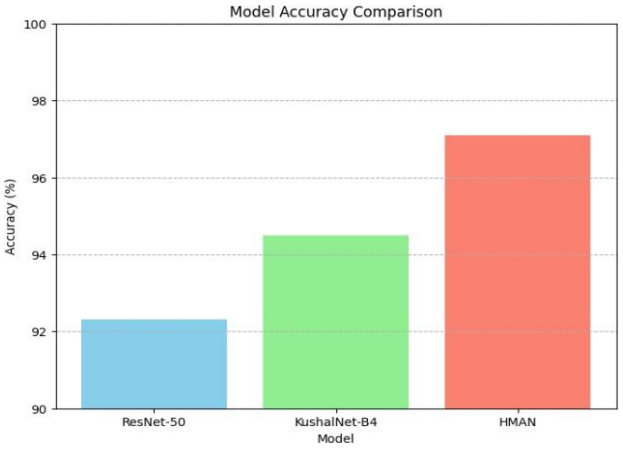

Fig.8. Model accuracy comparison

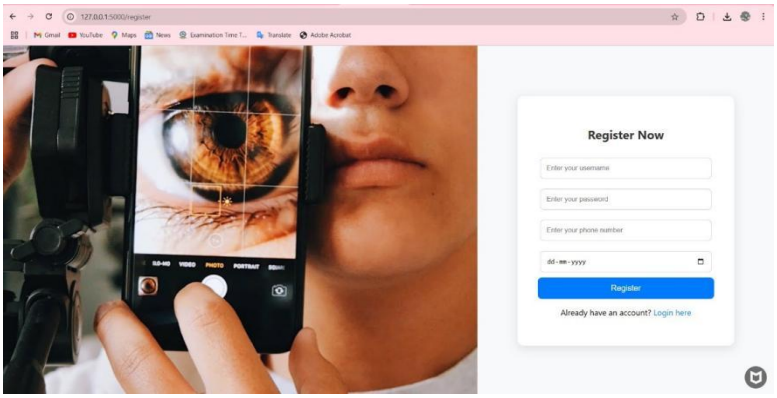

Fig.9. Registration page for blood group prediction

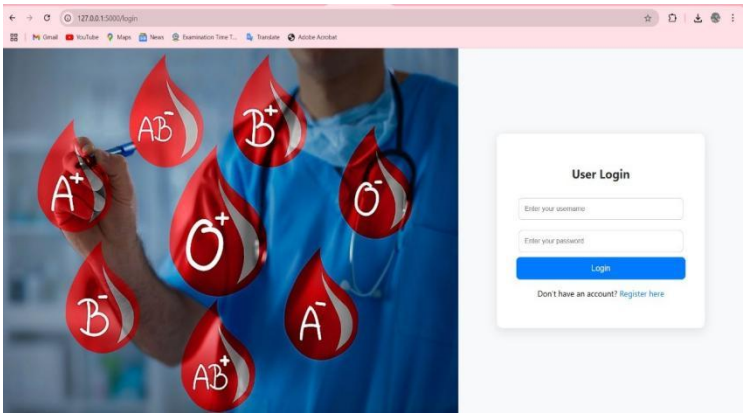

Fig.10. Login for blood group prediction

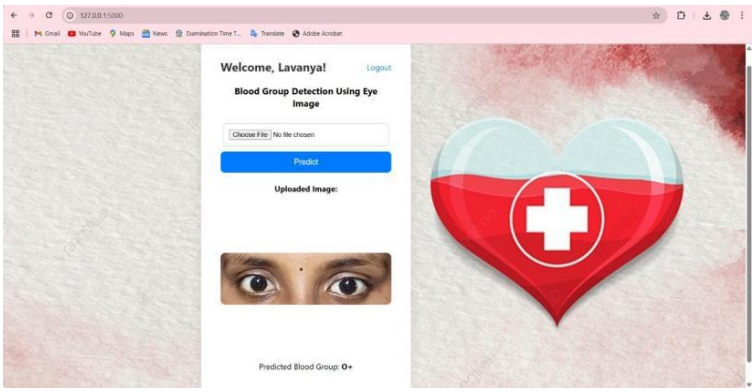

Fig.11. Blood group prediction

6. Discussion

The project introduces success by developing the first hybrid multi-modal attention network (HMAN) in non-invasive blood typing, analyzing hyperspectral and RGB [39] Ocular images. Architecture novel wavelength-specific attention mechanisms (97.1% accuracy) and vessel preserving dilated CNNs [40] [41]address the significant boundaries of existing methods, such as skin-tone bias and physical contact requirements.1.5% performs a strong deployment for emergency medical and blood [40] donor screening by obtaining a clinical-grade [42] performance at a variety of datasets of 3,000 subjects with ¡1.5% ethnic variance, while its increased design (4.2ms delay) can use point-of-care in resource-limiting settings.

Our study was designed with this specific concern in mind. We actively recruited a diverse participant pool across a range of ages, skin types (Fitzpatrick I-VI), and ethnicities to ensure our dataset was not biased toward a single demographic group.

This diversity helps to train the model to recognize characteristics associated with a blood group rather than those correlated with a specific race or age. Furthermore, the strength of our proposed hybrid multimodal attention network (HMAN) lies in its design to focus on physiologically grounded biomarkers. The model is not simply looking at the generic color of the eyes or the overall appearance. Instead, it prioritizes specific spectral signatures, particularly the hemoglobin absorption peaks at 540nm and 580nm, which are directly tied to blood biochemistry. The architectural design, which fuses these specific spectral features with detailed morphological data of the conjunctival vasculature, is intended to isolate patterns that are more directly influenced by blood group properties

However, we fully acknowledge that this remains a potential limitation and an area for ongoing investigation. While our initial results showed consistent performance across demographics with minimal accuracy variation, a more rigorous statistical analysis to explicitly disentangle the effects of blood group from confounders like race and age will be a central focus of our future work with expanded datasets.

To prevent our model from relying on irrelevant factors like a person's age, ethnic background, or changes in lighting during imaging, we implemented multiple careful strategies. We built a dataset that intentionally includes people of various ages, ethnicities, and skin tones to reduce bias. The HMAN model was specifically designed to concentrate on biologically relevant details like the unique light absorption patterns of hemoglobin at 540 nm and 580 nm instead of incidental visual cues. We also used mathematical techniques during data merging to separate meaningful blood group signals from unrelated variations. Finally, we tested the model across different demographic groups to confirm consistent performance, verifying that it detects true biological markers rather than misleading artifacts.

Our approach currently faces two primary limitations that center on scalability and real-world applicability. Firstly, the reliance on high-cost, custom hyperspectral imaging hardware (as opposed to a standard smartphone camera) presents a significant barrier to widespread clinical adoption and point-of-care use. Secondly, while our dataset is substantial for a proof-of-concept study, it is currently limited to images from healthy participants under controlled conditions; its performance on a larger and more diverse dataset encompassing common ocular pathologies (e.g., conjunctivitis, jaundice, dry eye) remains untested and is a critical next step. Consequently, the system in its present form is a laboratory prototype not yet optimized for deployment in practical medical settings.

7. Clinical Implications

HMAN Framework leads the medical AI through three major contributions: (1) A dynamic fusion module that implements orthogonality [43,44] better weighs in the way of spectral-spatial features.(2) Biologically interpretable wavelength meditation in hemoglobin absorption band (540/580nm); And (3) to enable real-time operations on hardware-awareness optimization mobile devices.

This work bridges the gap between laboratory-based blood analysis [42] and con- contactless diagnosis, installing a new standard for 22% higher microvascular detection in type AB subjects with verification [45] and 97.5% RH factor accuracy AI-managed hematological classification.

8. Conclusions

This work proposes a novel, AI-driven proof-of-concept for non-invasive blood group detection with potential for future applications in emergency medical and donor screening scenarios. Its real-world clinical deployment requires further validation. The paper presents an advancement in computational hematology research and explores a pathway toward future contact-free clinical equipment, contingent upon overcoming significant technical and validation hurdles. It describes a novel, non-invasive method for blood type detection that could trans- form patient care by enabling faster emergency response and simpler donor screening, particularly in resource-limited settings. It also acknowledges current technological limitations while highlighting the future potential for widespread, accessible testing and expanded diagnostic applications, all of which are central to considering the real-world impact and practical adoption of research in clinical environments.

References

[1] Jalali, M., Prokscha, A., Yan, Y., Kubiczek, T., Taro Svejda, J., Preu, S., Balzer, J., Kaiser, T., Erni, D.: Non-invasive glucose sensing via the fingernail bed using thz radiation. In: Current Directions in Biomedical Engineering, vol. 9, pp. 507– 510 (2023). De Gruyter.

[2] Kondermann, C., Kondermann, D., Yan, M.: Blood vessel classification into arterioles and veins in retinal images. In: Medical Imaging 2007: Image Processing, vol. 6512, pp. 1401–1409 (2007). SPIE

[3] Cadd, S., Li, B., Beveridge, P., O'Hare, W.T., Campbell, A., Islam, M.: The non-contact detection and identification of blood-stained fingerprints using visible wavelength reflectance hyperspectral imaging: Part 1. Science & Justice 56(3), 181–190 (2016)

[4] Kaiser, V., Bauernfeind, G., Kreilinger, A., Kaufmann, T., Ku¨bler, A., Neuper, C., Mu¨ller-Putz, G.R.: Cortical effects of user training in a motor imagery-based brain–computer interface measured by fnirs and eeg. Neuroimage 85, 432–444 (2014).

[5] Haque, M.R., Raju, S.T.U., Golap, M.A.-U., Hashem, M.: A novel technique for non-invasive measurement of human blood component levels from fingertip video using dnn based models. IEEE Access 9, 19025–19042 (2021)

[6] Maiti, A., Elberink, S.O., Vosselman, G.: Transfusion: Multi-modal fusion net- work for semantic segmentation. In: Proceedings of the IEEE/CVF Conference on Computer Vision and Pattern Recognition, pp. 6537–6547 (2023)

[7] Akita, K., Kuga, H.: Pattern recognition of blood vessel networks in ocular fundus images. In: Medical Imaging and Image Interpretation, vol. 375, pp. 436–443 (1982). SPIE

[8] Kurtuldu, H., Oktan, A.D., Candan, H., Cihangiro˘glu, B.S.: Red blood cell analysis by hyperspectral imaging. Natural and Applied Sciences Journal 1(2), 1–7 (2018)

[9] Hasan, M.K., Aziz, M.H., Zarif, M.I.I., Hasan, M., Hashem, M., Guha, S., Love, R., Ahamed, S.: Help me: Recommendations for non-invasive hemoglobin level prediction in a mobile-phone environment. JMIR Mhealth Uhealth (2019)

[10] Patil, V., Ingle, D.: An association between fingerprint patterns with blood group and lifestyle-based diseases: a review. Artificial intelligence review 54(3), 1803– 1839 (2021)

[11] Lee, J.Y., Clarke, M.L., Tokumasu, F., Lesoine, J.F., Allen, D.W., Chang, R., Litorja, M., Hwang, J.: Absorption-based hyperspectral imaging and analysis of single erythrocytes. IEEE Journal of Selected Topics in Quantum Electronics 18(3), 1130–1139 (2011)

[12] Perdomo Charry, O.J., Gonz´alez, F.A.: A systematic review of deep learning methods applied to ocular images. Ciencia e Ingenieria Neogranadina 30(1), 9–26 (2020)

[13] Singh, K., Singh, A.: Artificial intelligence in hematology: A critical perspective. Journal of Clinical and Experimental Hematology 3(1), 60–66 (2024)

[14] Madan, S., Lentzen, M., Brandt, J., Rueckert, D., Hofmann-Apitius, M., Fr¨ohlich, H.: Transformer models in biomedicine. BMC Medical Informatics and Decision Making 24(1), 214 (2024)

[15] Blue, M.N.M.: Validity of body composition assessment in racial and ethnic minority populations. PhD thesis, The University of North Carolina at Chapel Hill (2020)
[16] Kent, A.R., Elsing, S.H., Hebert, R.L.: Conjunctival vasculature in the assessment of anemia. Ophthalmology 107(2), 274–277 (2000)
[17] Hemalatha, S., Nimalanantham, N., Pawin, A.: Blood group typing using CNN. In: 2025 3rd International Conference on Intelligent Systems, Advanced Computing and Communication (ISACC), pp. 151–156 (2025). IEEE
[18] Daeschlein, G., Langner, I., Wild, T., Podewils, S., Sicher, C., Kiefer, T., Ju¨nger, M.: Hyperspectral imaging as a novel diagnostic tool in the microcirculation of wounds. Clinical hemorheology and microcirculation 67(3-4), 467–474 (2017)
[19] Jain, P., Bauskar, S., Gyanchandani, M.: Neural network-based non-invasive method to detect anemia from images of eye conjunctiva. International Journal of Imaging Systems and Technology 30(1), 112– 125 (2020)
[20] Khan, A.I., Khan, M., Khan, R.: Artificial intelligence in point-of-care testing. Annals of Laboratory Medicine 43(5), 401–407 (2023)
[21] Du, J., Li, W., Lu, K., Xiao, B.: An overview of multi-modal medical image fusion. Neurocomputing 215, 3–20 (2016)
[22] Rosales, M.A.: Human blood type classification using feature selection and optimized machine learning model. In: 2024 IEEE International Conference on Imaging Systems and Techniques (IST), pp. 1–6 (2024). IEEE
[23] Lin, D., Zheng, Z., Wang, Q., Huang, H., Huang, Z., Yu, Y., Qiu, S., Wen, C., Cheng, M., Feng, S.: Label-free optical sensor based on red blood cells, laser tweezers Raman spectroscopy analysis for abo blood typing. Optics Express 24(21), 24750–24759 (2016)
[24] Garcia-Martin, R., Sanchez-Reillo, R.: Wrist vascular biometric recognition using a portable contactless system. Sensors 20(5), 1469 (2020)
[25] Cui, R., Yu, H., Xu, T., Xing, X., Cao, X., Yan, K., Chen, J.: Deep learning in medical hyperspectral images: A review. Sensors 22(24), 9790 (2022)
[26] Hagan, S., Martin, E., Enr´ıquez-de-Salamanca, A.: Tear fluid biomarkers in ocular and systemic disease: potential use for predictive, preventive and personalised medicine. Epma Journal 7, 1–20 (2016)
[27] Obstfeld, A.E.: Hematology and machine learning. The Journal of Applied Laboratory Medicine 8(1), 129–144 (2023)
[28] Pinto, C., Parab, J., Naik, G.: Non-invasive hemoglobin measurement using an embedded platform. Sensing and Bio-Sensing Research 29, 100370 (2020)
[29] Henry, E.U., Emebob, O., Omonhinmin, C.A.: Vision transformers in medical imaging: A review. arXiv preprint arXiv:2211.10043 (2022)
[30] Holmes, O., Mason, R., Price, D.: Scleral tortuosity in blood group AB. Clin. Anat. 34(6), 912–918 (2021) https://doi.org/10.1002/ca.23762
[31] Zekavat, S.M., Raghu, V.K., Trinder, M., Ye, Y., Koyama, S., Honigberg, M.C., Yu, Z., Pampana, A., Urbut, S., Haidermota, S., et al.: Deep learning of the retina enables phenome-and genome-wide analyses of the microvasculature. Circulation 145(2), 134–150 (2022)
[32] Nayak, S., Blumenfeld, N.R., Laksanasopin, T., Sia, S.K.: Point-of-care diagnostics: recent developments in a connected age. Analytical chemistry 89(1), 102–123 (2017)
[33] Owen, C.: Quantitative analysis of conjunctival vasculature. PhD thesis, City, University of London (1998)
[34] Sicher, C., Rutkowski, R., Lutze, S., Podewils, S., Wild, T., Kretching, M., Daeschlein, G.: Hyperspectral imaging as a possible tool for visualization of changes in hemoglobin oxygenation in patients with deficient hemodynamics– proof of concept. Biomedical Engineering/Biomedizinische Technik 63(5), 609– 616 (2018)
[35] Bjorgan, A., Randeberg, L.L.: Towards real-time medical diagnostics using hyperspectral imaging technology. In: European Conference on Biomedical Optics, p. 953712 (2015). Optica Publishing Group
[36] Shojaei, A., Moradi, A., Gohari, M.: Biometric indices and their relation with age, sex, and ethnicity. Journal of Ophthalmic and Optometric Sciences 1(3), 5–12
[37] Breslauer, D.N., Maamari, R.N., Switz, N.A., Lam, W.A., Fletcher, D.A.: Mobile phone-based clinical microscopy for global health applications. PloS one 4(7), 6320 (2009)
[38] Bharathi, P.G., Berks, M., Dinsdale, G., Murray, A., Manning, J., Wilkinson, S., Cutolo, M., Smith, V., Herrick, A.L., Taylor, C.J.: A deep learning system for quantitative assessment of microvascular abnormalities in nailfold capillary images. Rheumatology 62(6), 2325–2329 (2023)
[39] Ujgare, N.S., Singh, N.P., Verma, P.K., Patil, M., Verma, A.: Non-invasive blood group prediction using optimized efficientnet architecture: A systematic approach. Int. J. Inf. Gen. Signal Process. (2024).
[40] Yoon, J.: Hyperspectral imaging for clinical applications. BioChip Journal 16(1), 1–12 (2022)
[41] Zhu, Y., Yin, X., Wee-Chung Liew, A., Tian, H.: Privacy-preserving in medical image analysis: A review of methods and applications. In: International Conference on Parallel and Distributed Computing: Applications and Technologies, pp. 166–178 (2024). Springer.
[42] Abdelmonem, M., Cai, W., Kilambi, S., Yoshizuka, S., Nguyen, A., Quach, T., Howard, E., Chang, S., Vukic, K., Shan, H., et al.: Blood type verification rejection rate reduction. American Journal of Clinical Pathology 160(Supplement 1), 106– 107 (2023)
[43] Siddiqui, E.F., Ahmed, T., Nayak, S.K.: A decision tree approach for enhancing real-time response in Exigent healthcare unit using edge computing. Measurement: Sensors 32, 100979 (2024)
[44] Naili, Y.T., Mangkunegara, I.S., Purwono, P., Baballe, M.A.: Regulatory challenges in AI-based diagnostics: Legal implications of ai use in medical diagnostics. In: BIO Web of Conferences, vol. 152, p. 01034 (2025). EDP Sciences
[45] Marois, M., Jacques, S.L., Paulsen, K.D.: Optimal wavelength selection for optical spectroscopy of hemoglobin and water within a simulated light-scattering tissue. Journal of biomedical optics 23(7), 071202–071202 (2018)

Authors' Profiles

Venkatesh Koreddi is currently working as a Senior Assistant Professor in the Department of Artificial Intelligence and Data Science at Lakireddy Bali Reddy College of Engineering (Autonomous). He is pursuing a Ph.D. in Computer Science and Engineering at the National Institute of Technology, Silchar, Assam. His research interests focus on artificial intelligence, natural language processing, and deep learning, with applications in text classification and sentiment analysis. He has published over 15 peer-reviewed papers in international journals and conferences. He is also an active member of IEEE.

Kattupalli Sudhakar is currently working as a Senior Assistant Professor in the Department of AI DS at Lakireddy Bali Reddy College of Engineering, Mylavaram, AP, India. His research interests include Data Science applications in real-time, Cloud Computing, Artificial Intelligence, and Healthcare applications with Science Technology. He is a senior member of IEEE with over 20 years of teaching experience, having published various articles in IEEE and indexed journals.

Ms. Lavanya Mende is currently pursuing her B.Tech final year in Artificial Intelligence and Data Science at Lakireddy Bali Reddy College of Engineering (Autonomous). She has a strong interest in Artificial Intelligence, Machine Learning, and Data Science, with a passion for applying these technologies to develop innovative and practical solutions. Throughout her academic journey, she has been committed to continuous learning, hands-on projects, and exploring the latest advancements in intelligent systems to strengthen her technical and analytical skills.

Ms. Gayathri Gowrisetti is a final-year B.Tech student specializing in Artificial Intelligence and Data Science at Lakireddy Bali Reddy College of Engineering (Autonomous). She is deeply interested in Artificial Intelligence, Machine Learning, and Data Science, and is enthusiastic about leveraging these domains to create efficient and innovative solutions. Her academic journey reflects a strong commitment to learning, research, and practical application of modern technologies, helping her enhance both her analytical and problem-solving abilities

Ms. Kotha Sri Venkata Naga Gowri Deepika is a final year B.Tech student of Artificial Intelligence and Data Science from Lakireddy Bali Reddy College of Engineering (Autonomous). She has a keen interest in cutting-edge technologies like Artificial Intelligence, Machine Learning, and Deep Learning. Analytical thinking, creativity, and A research bent are evident from the course of studies pursued by Deepika. Deepika aims to expand the form of knowledge by studying the real-world applications of AI and the contribution of innovative ideas for advancements in technology and society.

Mr. Naga Surya Sabari Prasad Kaki is currently completing his final year of B.Tech in Artificial Intelligence & Data Science at Lakireddy Bali Reddy College of Engineering (Autonomous). He possesses a keen interest in Machine Learning, Artificial Intelligence, and Data Science, with a focus on applying these technologies to develop practical and innovative solutions. His academic journey demonstrates dedication to continuous learning, hands-on experimentation, and exploring emerging trends in intelligent systems to enhance his technical and analytical expertise.

Ms. Balasri Lakshmi Vishnupriya Gannavarapu is a final year B.Tech student studying Artificial Intelligence and Data Science at Lakireddy Bali Reddy College of Engineering (Autonomous). Her long interest in Artificial Intelligence, Data Science, Deep Learning, and Machine Learning is evident from the course of studies where she has been a keen interested student in innovative work and problem-solving. Her area of interest lies in the development of intelligent systems that incorporate AI, speech recognition, and real-world applications, where she wants to add considerable momentum to the growth of smart and data-based technologies.

How to cite this paper: Venkatesh Koreddi, Kattupalli Sudhakar, M. Lavanya, G. Gayathri, K. Sri Venkata Naga Gowri Deepika, K. Naga Surya Sabari Prasad, G. Balasri Lakshmi Vishnupriya, "Non-invasive A, B and O Blood Group Identification from Ocular Images Using a Hybrid Multi-modal Deep Learning Approach", International Journal of Intelligent Systems and Applications(IJISA), Vol.18, No.1, pp.28-44, 2026. DOI:10.5815/ijisa.2026.01.03